



AIAA-2003-1199

**FURTHER EXPLORATION OF NOISE SOURCES IN A
MACH 1.3 JET**

*James Hileman, Edgar Caraballo, Brian Thurow and Mo
Samimy*

**The Ohio State University
Department of Mechanical Engineering
Columbus, OH 43210**

**41st Aerospace Sciences
Meeting & Exhibit
January 6 - 9, 2003 / Reno, NV**

Further Exploration of Noise Sources in a Mach 1.3 Jet

J. Hileman¹, E. Caraballo², B. Thurow³ and M. Samimy⁴

Department of Mechanical Engineering
Gas Dynamics and Turbulence Laboratory
The Ohio State University, Columbus, Ohio 43210

This work presents further effort on an on-going research project that aims to relate instantaneous large-amplitude features of the far acoustic field to the dynamic evolution and interaction of large-scale structures within the mixing-layer of ideally expanded, high-speed, high Reynolds number jets. It is believed that such information is essential for a better understanding of jet noise sources, and jet aeroacoustic modeling and control. The information presented here can be divided into three categories. The first part deals with the calibration of a 3-D microphone array that is used to locate instantaneous sources of sound within a high speed jet. The calibration was performed with both a plasma arc and a small fluidic device. Based on these results, the 3-D array can accurately locate noise sources possessing frequencies up to 10 kHz. The second part focuses on conditional sampling of the acoustic data at an observation location normal to the jet (90°) and one that is downstream of the nozzle exit (30°). The two locations have distinct phase averaged waveforms that correlate to the time scales of the turbulence structures that dominate the acoustic radiation in these two directions, i.e. the 30° waveform, where the radiation from larger turbulence scales dominate, has a larger temporal extent than the 90° waveform, where smaller scales dominate. The last part is a very preliminary examination of selected flow images using the Proper Orthogonal Decomposition (POD) technique. Based on data from the 3-D microphone array, flow images were divided into three categories for analysis: 1) those taken during the creation of intense sound, 2) images taken while the array was recording a period of relative quiet, and 3) a random selection of images. Image templates were created from the POD data, and these templates were then cross-correlated to individual flow images.

Introduction

The noise from the exhaust of jet engines has been a topic of interest for the last fifty plus years. Jet noise is a byproduct of the turbulence within the mixing layer of the jet, which forms due to the shear between the jet exhaust and the entrained ambient air. An in-depth understanding of jet turbulence has not been achieved, and as such, details about turbulence byproducts are even more limited. Because of this, the majority of progress in reducing jet noise has been a result of Lighthill's acoustic analogy,¹ a consequence of which is jet noise being proportional to the eighth power of velocity. Unfortunately, jet exit velocities cannot be reduced much further, and thus additional knowledge is required to achieve additional noise reductions. The research presented here is part of an ongoing project, which seeks to establish correlation between the dynamics of large structures within the jet mixing layer and the radiated acoustic far-field. Such knowledge could be instrumental to the development of new noise reduction schemes that

are specifically designed to modify dynamic behavior that is causing intense sound generation. Correlations have been performed on jet noise using flow measurements and a single microphone.²⁻⁶ This line of work differs from those in it implements a microphone array with non-intrusive flow measurements.

Simultaneous measurements have been conducted by the authors on a Mach 1.3 jet using an inline microphone array and temporally resolved flow visualization.⁷ The correlation was performed between the intense far-field noise radiation at the angle of maximum sound emission (30°) and images taken of the flow between 1 and 2 lengths of the potential core. Based on observation of flow images that were taken during noise emission and periods of relative quiet, three noise generation mechanisms were identified. These included: cross mixing layer interaction, large structure roll-up, and large structure tearing. Since these conclusions were based on observation, and as such were subjective, a part of the current work is devoted to an improvement to this

¹ Graduate student, OSGC Fellow, member AIAA

² Graduate student, DAGSI Fellow, member AIAA

³ Graduate student, NDSEG Fellow, member AIAA

⁴ Professor, Associate Fellow AIAA, corresponding author

Copyright © 2003 by James I. Hileman. Published by the American Institute of Aeronautics and Astronautics, Inc. with permission.

process using Proper Orthogonal Decomposition (POD). POD has been used extensively to identify the most energetic structures/modes in various flows. It has been used with data from high-speed jet simulations⁸⁻⁹ as well as low speed jet experimental data¹⁰⁻¹³. Kopp et al.¹⁴ used the first two POD modes to create templates for pattern recognition in a low speed wake created by flow over a cylinder. A similar approach will be taken in this work. POD will be used to create templates of flow features within the flow during certain acoustic states (as determined by a 3-D microphone array). These templates can then be used to identify flow features during sound emission.

The objective of this work is the further advancement of the research conducted in references 7, 15-16. The paper covers three disparate, but related subjects. The first segment is devoted to the validation of the 3-D microphone array that was initially described in reference 16 and used for noise source location in tabbed jets in reference 17. Emphasis is placed on determining the range of operation for the array in the frequency domain. The second section delves into conditional sampling of the acoustic data. Previous work was devoted to the temporal analysis of the acoustic field of the Mach 1.3 at a 30° observation location. This is being extended to analysis at a 90° observation angle as well. The last section is devoted to a preliminary analysis where POD is used to analyze flow images that were simultaneously acquired with noise source measurements from the 3-D microphone array are presented.

Experimental Arrangement

This section describes the noise source location technique, the temporally resolved flow visualization, as well as the manner in which they were used

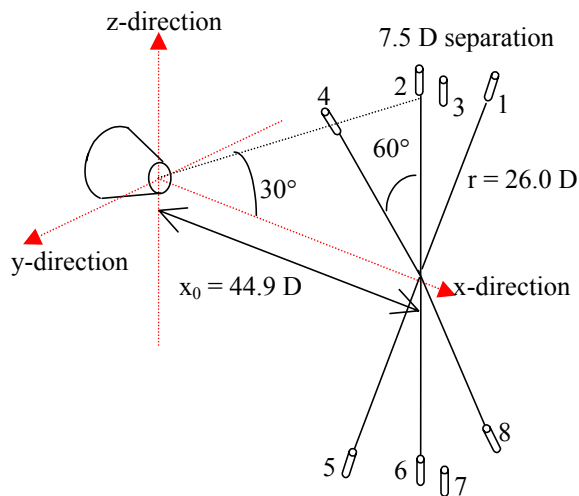


Figure 1: Schematic of the 3-D microphone array.

simultaneously. All of the experiments were conducted in the optically accessed anechoic chamber of the Gas Dynamics and Turbulence Laboratory of the Ohio State University. The jet had a Mach number of 1.28, diameter of 2.54 cm (1 inch), and a Reynolds number of 1.08×10^6 . Details of the facility can be found in references 7 and 15.

3-D Microphone Array

The purpose of this work is to relate the *dynamics* of large turbulence structures to the emission of sound; hence a unique approach is required. Conventional methods of noise source localization that rely on analysis of the frequency domain will not work. What is needed is a temporal domain analysis where the origin of individual sound events can be determined. Based on this unique need, a novel approach was taken in the design of an acoustic array. It works by measuring the phase lag of individual sound events between microphones in space. With this phase lag information and the geometry of the array, a sound origin is determined for every acoustic event that exceeds a set amplitude threshold. The present 3-D microphone array/analysis algorithm is a third-generation design that

measures the time of flight difference between an individual acoustic peak being recorded by various microphones in space. The first generation array consisted of two microphones aligned with the x-direction, separated by 5 nozzle exit diameters, and placed at the 30° location. This array was used with dual pulse flow visualization in reference 15. The second generation array expanded the number of microphones to four with a total aperture of 6 nozzle exit diameters. It was used in conjunction with real-time flow visualization in reference 7. The third generation design has six azimuthally distributed microphones (microphones 1, 2,



Figure 2: Photograph of the 3-D microphone array within the optically accessed anechoic chamber of the Gas Dynamics and Turbulence Laboratory.

4-6, 8 in Figure 1) to determine the cross-stream plane origin and two sets of inline microphones (microphones 2&3, 6&7) to determine the streamwise origin. Figures 1 and 2 show a schematic and photograph of the array. Further details of the array and the associated noise source location algorithm can be found in reference 16.

Temporally resolved flow visualization

The mixing layer of the jet was visualized in real-time over periods of 128 μsec . Condensation of moisture from the ambient air within the jet mixing layer was used to visualize the flow and to track the evolution of large-scale turbulence structures within the jet. This temporally resolved flow visualization was made possible by a pulse burst laser / high frame rate camera system. The pulse burst laser operates at 532 nm with about 15 mJ of power per pulse. The increase in power from previous publications was due to the addition of a fifth amplifier and a phase conjugate mirror.¹⁸ The number of laser pulses was set at 17 with 8 μsec separation between pulses. A Dalsa model 64K1M camera was used to acquire the images. Further details on the pulse burst laser / flow visualization technique can be found in reference 19. The temporal resolution of these image sets was used in this work to obtain an image set that was taken as close to the peak sound production as possible.

Simultaneous Measurement

The two previously described measurements, noise source localization and temporally resolved flow visualization, were performed simultaneously to acquire four hundred sets of data. In each set, seventeen temporally resolved flow images were taken a set period of time after the start of the acquisition of 8192 data points (8.192 ms of data) with the 3-D array. The pulse burst laser system was located outside of the anechoic chamber, while the Dalsa camera was inside of the chamber perpendicular to the streamwise laser sheet. The camera was covered in acoustic foam as were all other exposed surfaces. Apparent noise source origins were computed for every acoustic event with amplitude in excess of 1.5 times the standard deviation. Equations 8 and 9 from reference 15 were used to compute where each of these acoustic events would be during the simultaneously acquired flow images. Simultaneous measurements using the first and second generation inline microphone arrays with dual pulse flow visualization and temporally resolved flow imaging are described, respectively, in references 7 and 15.

Part I: 3-D Array Validation

Since the 3-D array is a unique design, extra steps have been taken to confirm its ability to determine the location of noise sources. Two different noise generators were used to test the ability of the array to locate noise sources. The first was an AC plasma (spark) generated between a pair of wires powered at varying

frequency. The other was a Hartmann tube fluidic actuator (HTFA),²⁰ which is also referred to as a powered resonance tube in the literature.²¹ The sound from the plasma was approximately a point source, in fact a short line source that was about 3 mm in length (0.1 jet diameter), while that from the HTFA was distributed over a small area of moving fluid.



Figure 3: Photograph of the plasma arc used for 3-D array calibration.

The plasma arc was created by applying a sinusoidal voltage of 15 kV across a small gap between two electrodes. The plasma arc setup is shown in Figure 3. By varying the input sine wave, the frequency with which the arc fired varied from 1 to 20 kHz. With this variation, the plasma arc was also used to analyze the ability of the array to locate noise sources of varying frequency. The plasma arc was located at $[x/D, y/D, z/D] = [8, 0, 0]$ in all of these experiments. For each case, at least 0.15 seconds of data were analyzed, which yielded thousands of individual noise source locations for each of the selected frequencies. Figures 4 through 6 show the average and standard deviations for the three spatial coordinates of the calculated noise source locations. The standard deviation gives a good indication of the acceptable frequency range of operation of the array. Since the source is a stationary point, there should be minimal deviation among the calculated sound origins. The standard deviation of the x-component of the noise source location significantly deviates from zero above 10 kHz, the z-component above 12 kHz, and the y-component above 14 kHz. These locations also match the frequencies where the means begin to deviate from the actual plasma location (these are marked by the horizontal lines in the three figures). Based on this validation, the array is capable of accurately locating noise sources with frequency content up to 10 kHz.

For frequencies of 3 and 12 kHz, the plasma arc was precisely located with respect to the nozzle exit. The desired location was measured to within approximately 1 mm (0.04 jet diameter) of the centerline of the jet, and

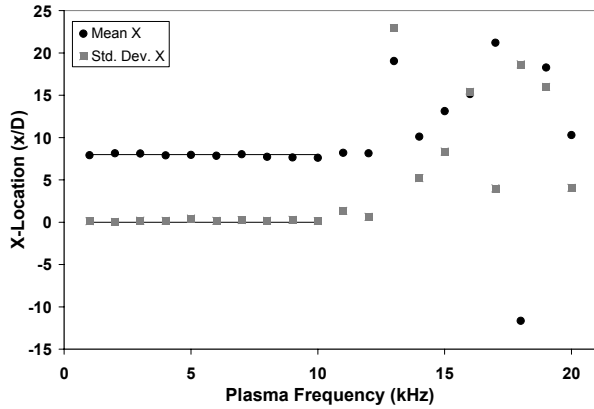


Figure 4: Predicted x-location of the plasma arc using the 3-D array for varying plasma firing frequency.

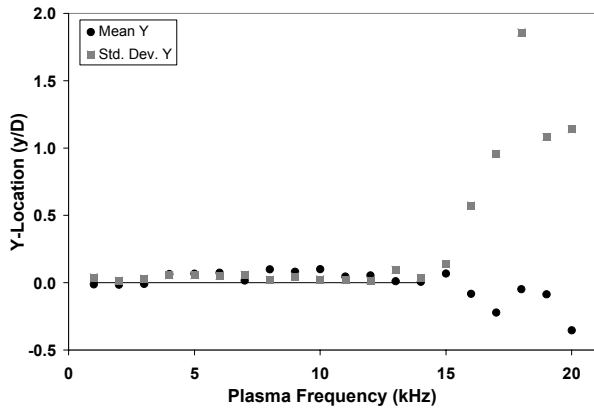


Figure 5: Predicted y-location of the plasma arc using the 3-D array for varying plasma firing frequency.

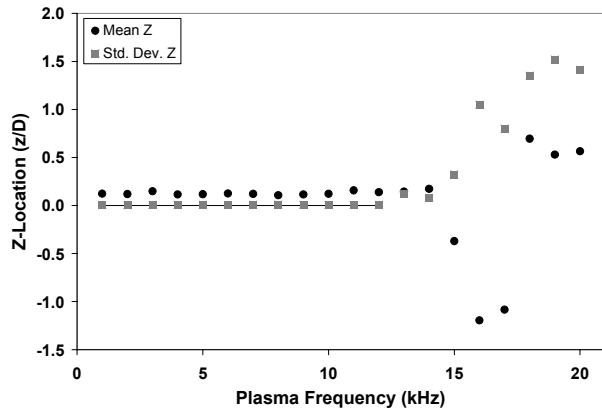


Figure 6: Predicted z-location of the plasma arc using the 3-D array for varying plasma firing frequency.

then two lasers were used to mark this point in space. The electrodes that were used to create the plasma arc were placed to straddle the two laser beams. For the

lower frequency (3 kHz), the mean of the calculated noise origins was $[x/D, y/D, z/D] = [8.17, 0.02, 0.18]$, while for the higher frequency (12 kHz) the mean was $[x/D, y/D, z/D] = [8.50, 0.01, 0.16]$. The x-component was expected to be in error for the higher frequency as this is beyond the resolvable frequency for the array and the y-component deviation is acceptable. The offset in the z-component likely originates within the array setup. The most likely explanation for the small discrepancy in the z direction is that the center of the array was offset from the centerline of the jet by a small distance. The 3-D array projects noise sources onto a set of orthogonal coordinates where the x-coordinate passes through the center of, and is perpendicular to, the plane that is formed by the azimuthal distribution of microphones. If the center of the ring were offset from the center of the nozzle, then there would be an equal offset in the location of each noise source from the jet centerline. The previously mentioned noise locations showed a discrepancy of 5 mm (0.2 jet diameter) from the actual plasma arc. This should not be surprising for such a large array configuration and this value was then used as a correction in the noise processing codes. It was implemented by moving each microphone down 5 mm in the noise location codes (-5 mm z-direction). The initial setup of the 3-D array, which was reported in reference 16, had a correction of -4.3 mm in the y-direction and by -7.1 mm in the z-direction.

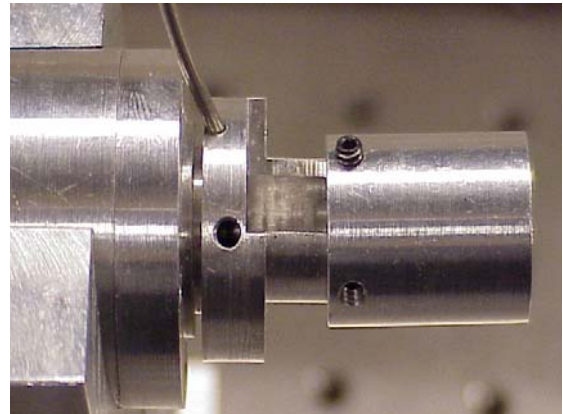


Figure 7: Photograph of the HTFA used for 3-D array calibration.

As mentioned previously, an HTFA was used as an additional calibration. A Hartmann tube consists of a small underexpanded jet and a closed-ended tube, which is aligned with the jet. The open end of the tube is placed within a compression region of the underexpanded jet.²² An HTFA is created by placing a cylindrical shield between the nozzle and the tube that covers a large portion of the open area.²¹ The HTFA used for the validation is based on the design described in reference 20 and shown in Figure 7. The converging nozzle of the HTFA had an exit diameter of 6 mm and the opening of

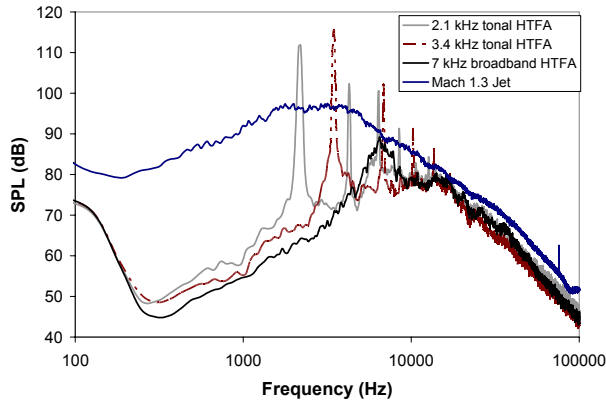


Figure 8: Acoustic spectra from three configurations of the HTFA along with the spectra from the Mach 1.3 jet.

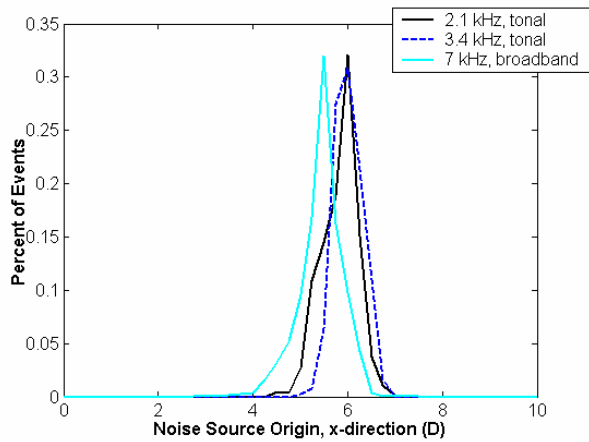


Figure 9: Noise source probability distributions for the x-direction for the three HTFA configurations.

the HTFA was a square with 8 mm sides. By varying the length of the tube, the resonant frequency of the HTFA can be varied. Three tube lengths were used for the current validation. Two of the tubes created a pure tone, either 2.1 or 3.4 kHz; while the third tube created broadband acoustic radiation centered on 7 kHz. The spectra for the three cases, as well as the Mach 1.3 jet, are

given in Figure 8. All of these spectra were taken from the same microphone of the 3-D array. The opening of the HTFA was 4.9D downstream of the origin, centered on the nozzle exit plane, with air exiting the HTFA along the jet centerline.

All of the noise events exceeding 1.5 times the standard deviation were examined to determine the origin of the acoustic radiation for the three cases. The aforementioned z-component correction was applied to the microphone locations prior to processing. The probability density distributions in the x-direction for all three cases have been plotted in Figure 9. The majority of the noise sources were located within a 75 mm region

that starts at the rear of the HTFA. This matches the flow visualization images of a similar HTFA,²⁰ which showed significant vortical flow activity over the entire opening of the HTFA that extends significantly away from the opening. The distributions do vary slightly; the non-resonant case (7 kHz broadband) is distributed between 4 and 6.5 x/D while the two resonating, tonal cases are between about 5 and 7 x/D. The cross-stream distributions are given in the forms of 2-D probability density plots in Figures 10 through 12 that cover a range of 0.5D (12.7 mm). The bin size is 0.05 D in both directions. All three figures show distributions that are within 0.1 D of the z-axis, but have an offset in the negative y-direction. This offset matches the location of the edge of the HTFA opening where the flow images showed significant vortical flow.²⁰ Hence, the area of noise generation again matches the area of expected noise generation (these are the regions of significant vorticity as observed in reference 20).

These results are quite encouraging. The 3-D array was able to locate a point noise source (plasma arc) with a primary frequency that varied from 1 to 10 kHz. The plasma arc was then used as a calibration to determine the offset between the center of the 3-D array and the apparent jet centerline. The 3-D array was also able to determine the area of vortical flow from a small fluidic device (HTFA) regardless of whether it was creating a pure acoustic tone or broadband acoustic

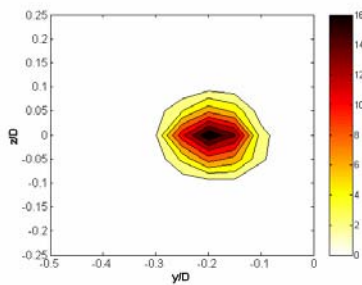


Figure 10: Cross-stream distribution of noise sources for the 2.1 kHz HTFA

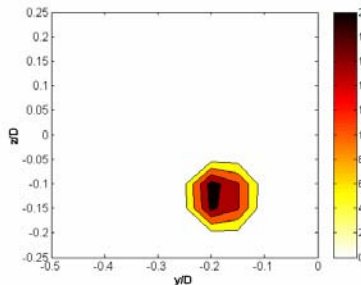


Figure 11: Cross-stream distribution of noise sources for the 3.4 kHz HTFA

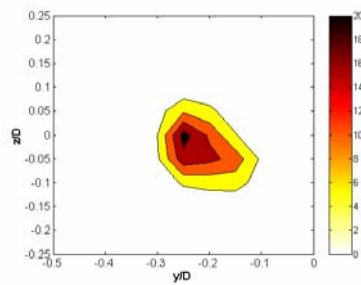


Figure 12: Cross-stream distribution of noise sources for the 7 kHz HTFA

radiation. At this point, the 3-D array was deemed ready for use in determining the noise emitting region from a high-speed jet.

Frequency Filtering and Noise Distribution

Based on the plasma arc noise distribution data, the array can only resolve frequencies below 10 kHz. As such, data taken with this 3-D array configuration should be low-pass frequency filtered at 10 kHz prior to analysis for noise origins. To this end, a fifth order Chebyshev type I digital filter was applied to the raw acoustic data from the Mach 1.3 jet. The data were normalized by their standard deviation after filtering, and then processed for noise source calculation. Several low-pass frequencies were used to explore the effect of frequency filtering on the distribution of noise sources. One should keep in mind that the results for frequencies above 10 kHz might be in error as evidenced in the plasma arc data. Four filtering frequencies (6 kHz, 10 kHz, 20 kHz, and no filtering) were used to create the distributions shown in Figure 13. These plots were created by determining the apparent origin of noise events that were recorded by microphone 2 of the array with a magnitude in excess of 1.5 standard deviations. The data set consisted of 400 sets of 8,192 samples taken at a sampling rate of 1 MHz. The effect of filtering is relatively small, but consistent with the microphone array work of references 23-25 where higher frequency noise was found to originate closer to the jet exit. This is shown by the decrease in the mean value with increasing frequency content (the results are low-pass filtered, hence the higher frequency settings contain a larger range of frequencies). As mentioned previously, above 10 kHz the array predicted noise origins that did not match the location of the plasma arc, and as such, 10 kHz was the selected frequency for low-pass filtering. Figure 14 shows the cross-stream probability distribution plot of noise sources with the 10 kHz low-pass filter. The bins that were used to create the plot are 0.05 D on a side. The means for the noise source

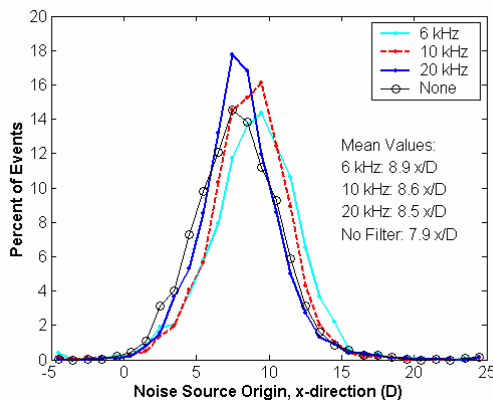


Figure 13: Downstream distribution of noise sources with varying low-pass frequency filtering.

distribution are 8.6 x/D, 0.2 y/D and 0.0 z/D.

Part II Conditional Sampling of Acoustic Data

Much of the work in references 7 and 15 was focused on the maximum noise emission direction of 30° where the acoustic radiation from large structures is known to dominate. Various acoustic measurements were taken to ascertain the average character of the acoustic emission in the time domain. These measurements included an average waveform that is representative of the large amplitude sound events and an analysis of the percent of time a microphone was recording various types of acoustic emission. These measurements were repeated for an observation direction of 90° where acoustic radiation from smaller scales should dominate. Throughout, a large amplitude sound event is defined as an acoustic peak that exceeds a set threshold in the time domain. Furthermore, the acoustic data from the 30° and 90° observation directions have both been normalized by their respective standard deviations before these analyses were conducted.

One means of analyzing acoustic data is to phase average all of the acoustic events that exceed a set threshold in the time domain. This was originally done for the acoustic data from a Mach 1.3 jet for threshold levels of 1.5σ and 2.0σ at the 30° location to create the average acoustic waveforms in reference 7. Another way of setting the threshold criteria would be to examine all acoustic events that have a magnitude within a set band (e.g. 1.5σ - 2.0σ). The waveforms shown in Figure 15 below were created by accepting acoustic events for various bands for the 30° location. This was then repeated for the 90° location to create Figure 16. Data for the waveforms extends from 1 ms before the main peak to 1 ms afterward; however, only the central portions are given in the two figures. It is important to note the difference in the scales of the two figures (1 ms versus 0.2 ms). It is also worth noting that the threshold

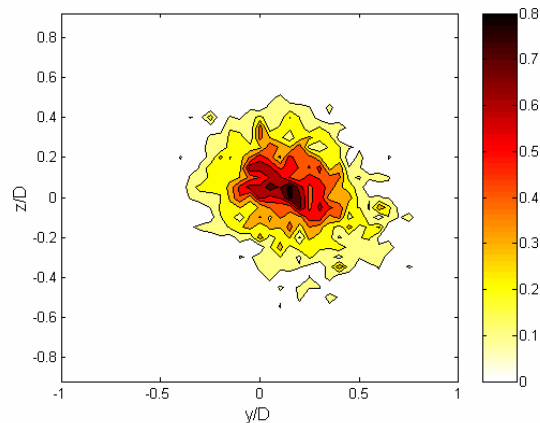


Figure 14: Cross-stream distribution of noise sources with a 10 kHz low-pass filter.

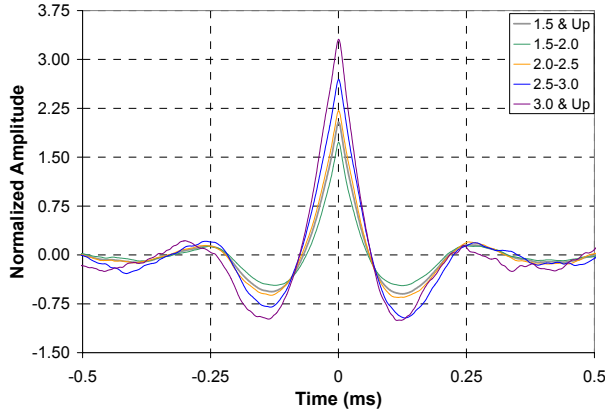


Figure 15: Average waveform for various thresholds for the 30° observation location. Data normalized by standard deviation for 30° location.

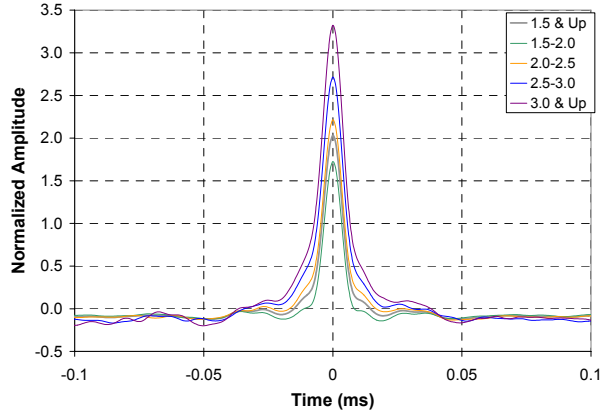


Figure 16: Average waveform for various thresholds for the 90° observation location. Data normalized by standard deviation for 90° location.

band does not significantly affect the waveform shape (only the magnitude of the main peak and side lobes).

The difference between the waveforms for the two locations is obvious. The 30° location has a wave shape with distinct side lobes whereas the 90° location is dominated by a single narrow peak without any side lobes. The 30° waveform bears a strong resemblance to the acoustic field generated by the interaction (leapfrogging) of two ring vortices where the peak sound emission was found to coincide with the two vortices passing through one another.²⁶⁻²⁹ The time scales of the waveforms correlate well with the structure scales that are known to dominate the production of acoustic radiation in these two directions. The smaller scales, which have acoustic radiation that dominates at the 90° location, have a shorter time scale than the larger scales that radiate in the 30° direction. This matches the dramatic difference in the widths of the waveforms shown in Figures 15 and 16. In reference 7, the spectrum

from the 30 degree waveform was shown to be quite similar to the overall jet spectrum taken at the same location. Although it is not shown here, the 90 degree waveform also has a spectrum that possesses the same shape as the overall jet spectrum taken from the same location. Apparently a lack of side lobes correlates to the flat spectrum that is observed at locations normal to the jet exit. In a related note, the waveforms from tabbed jets do have side lobes that are similar to those in Figure 15. For the 1 inch diameter jet under study here, they correspond to a broad spectral peak between 10 and 40 kHz, which is observed in the overall spectrum [these results will be presented at the 9th AIAA/CEAS Aeroacoustics Conference in May 2003].

The average acoustic waveforms possess a strong resemblance to the autocorrelation of the acoustic data. Figures 17 and 18, below, compare the average waveform and the autocorrelation of the 30° and the 90° directions data, respectively. The acoustic waveform has

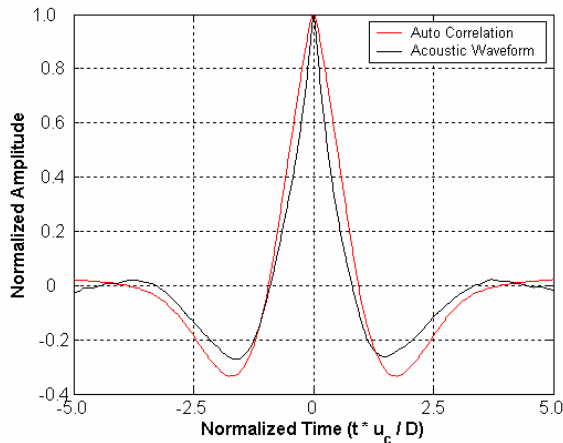


Figure 17: Comparison of the average waveform and autocorrelation for the 30° observation location.

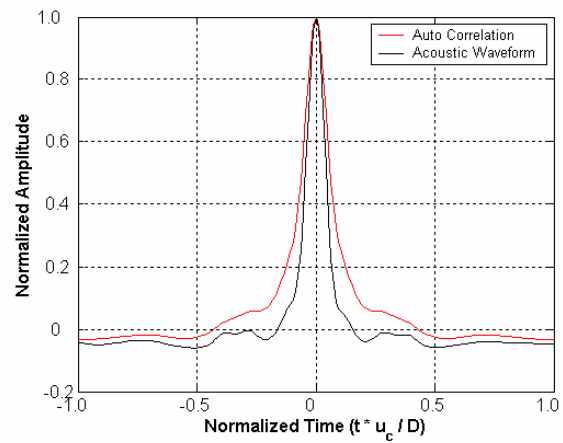


Figure 18: Comparison of the average waveform and autocorrelation for the 90° observation location.

Location	Creating event >1.5 σ	Creating event >2.0 σ	Relative quiet for 0.5 ms	Relative quiet for 1.0 ms	Periodic acoustic emission
$\theta = 30^\circ$ (downstream of nozzle exit)	51%	26%	20%	5%	15%
$\theta = 90^\circ$ (normal to nozzle exit)	52%	29%	0%	0%	33%

Table 1: Percent of time the jet was in various modes for 30° and 90° observation locations.

been normalized to have maximum amplitude of one, while an autocorrelation has a maximum of one by definition. While their amplitudes have been artificially matched, the similarity in their shapes likely results from their inherent similarity in the frequency domain. The acoustic frequency spectrum could have been created from the autocorrelation of the acoustic signal; while the acoustic waveform has been shown to possess the frequency content of the signal. Hence, they have similar frequency content, and as such would likely have similar temporal content.

Conditional sampling of the acoustic data was also performed to ascertain how often large amplitude events are being created in the 90° direction, which can then be compared to data taken at the 30° direction. Unlike other results presented in this work, this data was taken with 100 kHz low-pass frequency filtering. Three types of events were recorded: (1) percent of time the microphone was recording an acoustic event above a threshold level, (2) the percent of time the microphone went without recording an acoustic event above 1.5 σ over two different lengths of time, and (3) the percent of time the microphone was recording three or more successive acoustic peaks that all exceeded 1.5 σ with a set period between consecutive peaks. The two time lengths in Table 1 correspond to a large structure convecting 5 or 10 jet diameters if it were traveling at the measured convective velocity of 270 m/s.¹⁹ The periodic acoustic emission was required to have a frequency content between 1 and 10 kHz, and the time period between a successive peak and valley within the peak/valley set had to be within 33 percent of the other periods. This analysis was summarized for the 30° location in reference 15 for a Mach 1.3 jet, and in reference 17 for tabbed, Mach 1.3 jets. The results for the two locations are summarized in Table 1 where the data for 30° was taken from reference 17.

This temporal analysis shows the percent of time an observer would hear large amplitude (large in comparison with the acoustic data at the respective observation location) noise events does not change with position, but they are occurring more sporadically at the 30° location. This is evidenced by the complete lack of relative quiet periods at 90° and the dramatic increase in periodic events. Based on these results, the jet appears to

be nearly continuously generating sound in the sideline direction. This should not be surprising as the frequency content of the 90° location is spread over a wider range than that at the 30° location, which is dominated by a broadband peak centered on 3 kHz, ($St_D = 0.2$).¹⁵

Part III: POD & Pattern Recognition of Select Flow Images

To obtain images that captured noise generation events and periods of relative quiet, four hundred sets of temporally resolved flow visualizations were taken with simultaneous noise source localization using the 3-D microphone array. These data were low-pass filtered digitally at 10 kHz using the aforementioned Chebyshev filter. The acoustic data from the front inline microphones at the top and bottom of the array (mics 2 and 6) were analyzed to find all acoustic peaks that exceeded 1.5 times the standard deviation. Noise source calculations were then performed on both sets of acoustic peaks. This gave a set of noise sources that was based on large events reaching the bottom of the array and one based on events reaching the top. The distribution for the top microphone was shown in Figures 13 and 14. The acoustic data from microphones 2 and 6 were also analyzed to determine periods of relative quiet as recorded by the microphones on opposing sides of the jet. This analysis was performed to gather images that captured one of three activities: 1) both sides of the array recorded a large amplitude acoustic event that originated from a single part of the jet, 2) one side of the array recorded a large amplitude acoustic event while the other was recording a period of relative quiet, and 3) both sides of the array were recording a period of relative quiet. Unfortunately, this data set was not large enough to record a statistically significant number of types (1) or (2). Only three instances of noise generation originating from one part of the jet, but reaching both sides of the array, and five instances where one side of the jet was recording relative quiet while the opposing side observed sound generation were captured in the four hundred images. However, a large number of type (3) were recorded. We will be using these images to construct POD bases to create unique templates that capture each type of event. For POD a statistically significant number is required and three to five images definitely will not suffice. For this reason, images that apparently captured

noise emission will be examined without regard for what was occurring on the opposite side of the array and there will be no analysis of images where both sides of the array recorded a sound event.

Proper Orthogonal Decomposition

Previous work performed by the authors has relied on the subjective analysis of flow image sets that were taken during apparent noise emission or relative quiet as recorded by the microphone array. Each set of images were examined visually to determine what they had in common. This subjective method has been useful in the analysis of the flow images, but it could be improved upon. What is needed is an objective method to determine what is common to any set of images. Proper Orthogonal Decomposition will be used for this purpose. This section presents preliminary results in the development and use of POD for pattern identification in flow images.

The POD technique has been used extensively to decompose complex flow fields into a few modes that capture the dynamically significant features of the flow. POD is generally used with measured or numerically simulated flow data. At this stage of this research project, quantitative flow measurements have not been made, and all that is available for POD analysis are flow images. As such, the variable that is being used for spatial correlation will be image intensity. Each flow image was normalized by a high-order polynomial fit so the maximum intensity of any column would be equal to one, and then the mean of four hundred images was removed from each image. Hence, the variable being considered is intensity deviation from the mean. The flow images were taken in temporally resolved sets of 17 images, but the real-time aspect was not directly employed. The set of images did allow for the analysis of flow images that were taken within 10 μ sec of the peak sound emission. This was done by choosing the frame

that was taken closest to peak sound emission.

The POD employed here uses the snapshot method of Sirovich,²⁹ which is more appropriate for data with high spatial resolution. The application of the technique follows the approach used by Caraballo et al.^{9, 30} in their reconstruction of the velocity field of a Mach 1.4 jet and Mach 0.38 cavity flow using numerically simulated data, respectively. In this case, the reconstruction will be of flow images using their intensity. Flow images were analyzed with POD to obtain the first two modes. These two modes were then used to reconstruct each flow image that was in the original set, and these were ensemble averaged to get a template for the structure dynamics.

As was done in references 7 and 15, flow images were selected for POD analysis based on the data set measured with the 3-D microphone array. Three types of acoustic events were analyzed, which led to three templates for pattern matching:

1. The center microphone on one side of the array (either 2 or 6) recorded an acoustic event that has an apparent origin within a set region of the jet and the emission occurred during a flow image set. These events were created between 8.5 and 10.5 x/D and had a magnitude in excess of 2.0 standard deviations. This set consisted of 15 flow images.
2. Flow image sets were taken while both sides of the array (microphones 2 and 6) were recording a period of relative quiet (no acoustic peaks in excess of 1.5 standard deviations) between the times of 3.5 and 3.9 ms, over a period in excess of 0.5 ms. This set consisted of 15 flow images.
3. Random selection of 15 flow images.

We understand that 15 images will not constitute a convergent basis. In other words, different random sets

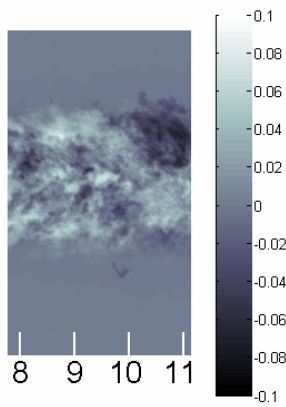


Figure 19: Noise generation template; 23.9% of the total intensity variance was captured.

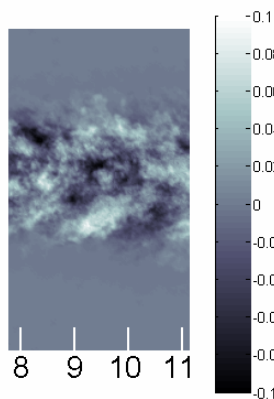


Figure 20: Relative quiet template; 22.7% of the total intensity variance was captured.

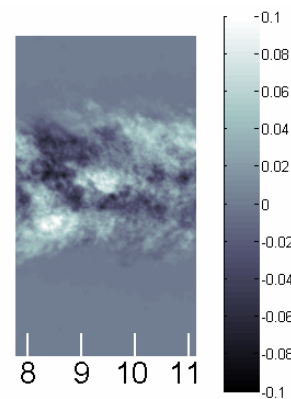


Figure 21: Random template; 28.1% of the total intensity variance was captured.

of 15 images yield bases that vary. A larger data set would alleviate this problem by providing more images for basis construction. This will be addressed further in the next paragraph.

The first two POD modes yielded about 25% of the intensity variance that was contained in the original images. Since one of the criteria in the selection of the images was noise generation within a set region, only a portion of each image was used for POD analysis. Based on the possibility that a large region could be responsible for the creation of sound, the area between 7.8 and 11.2 x/D was chosen for analysis. The three templates are shown in Figures 19 through 21, flow is from left to right and distance from the nozzle exit is given in number of jet diameters at the bottom of the templates. One has to remember that these figures show the deviation of the intensity from the mean, which is given in Figure 22 (this figure extends from 5.1 to 11.2 x/D). The three templates have been plotted on identical gray scale levels to show the differing levels of fluctuation from the mean image. To achieve the identical gray scale levels, several sets of random images had to be processed for POD analysis. The intensity fluctuations varied greatly depending on the data set. For some sets, all of the fluctuations were below 2%, while others achieved fluctuations in excess of 15%. Thus, this random template must be regarded with caution as another set of random images might yield a different template. We must reiterate that this is a very preliminary analysis and a work in progress.

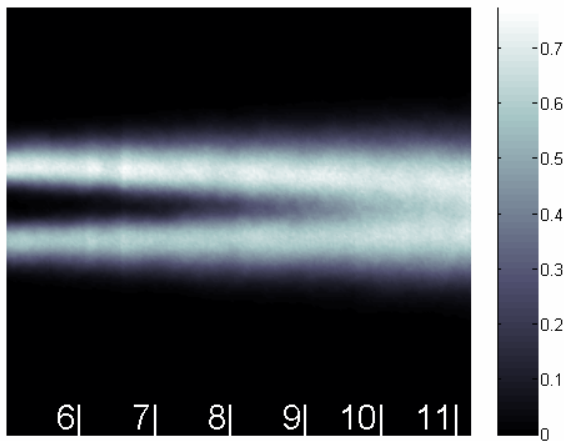


Figure 22: Mean flow image.

The noise generation template has intensity fluctuations that are generally positive (the white coloration), while the relative quiet template has alternating regions of positive and negative intensity fluctuations. Since the intensity of a flow image is a reflection on the amount of mixed fluid present, it stands to reason that regions where the fluctuation in the intensity is positive correspond to the location of larger turbulence structures and those that have negative

intensity fluctuations correspond to a relative lack of large structures. With such an interpretation of intensity fluctuations in mind, the relative quiet template has a lack of very large coherent structures since the regions of uniform intensity fluctuation are relatively small compared to the width of the jet. The large regions of positive or negative intensity fluctuations in the noise generation template could be interpreted as the jet possessing significant regions of coherent motion in the mixing layer since these regions are much larger than those of the relative quiet template. This random template appears to fall some where between the two in terms of the size of fluctuating regions. Future work should improve upon the templates as we will attempt multiple approaches in the construction of the POD bases.

Pattern Recognition

Each of the templates was correlated to a selection of images to determine if indeed they have captured the dynamics of noise generation. The method for comparison was kept quite simple for this preliminary examination. A two dimensional correlation was performed between each of the templates and all of the images that were used to create the three templates as well as an additional fifty randomly selected images (giving 285 correlation values in all). These correlation levels were then averaged based on the three templates and the set of randomly selected images to yield 12 values. The two-dimensional correlation coefficient, r , between the template and individual images was computed using:

$$r = \frac{\sum_m \sum_n (A_{mn} - \bar{A})(B_{mn} - \bar{B})}{\sqrt{\left(\sum_m \sum_n (A_{mn} - \bar{A})^2\right)\left(\sum_m \sum_n (B_{mn} - \bar{B})^2\right)}}$$

where \bar{A} and \bar{B} denote the means of A , and B , which are the template and image respectively. The individual correlation coefficients were then averaged to yield the values given in Table 2. The numbers in parenthesis give the number of images that were used to create each template as well as the number of correlation coefficients that were averaged to get the value listed.

As expected, the highest coefficients came from the templates and the individual files that were used to construct them (values along the diagonal). The next highest level came from the random template and the set of fifty random images (5.9%). The rest of the values are lower than the random correlation. This would seem to indicate that there is a higher correlation between a random template and other random images than there is between any of the templates and the files that were used to create a different type of template. These data are

	Noise Generation (NG) Template	Relative Quiet (RQ) Template	Random Template
Files used for NG-Template (15)	11.2%	0.9%	0.3%
Files used for RQ-Template (15)	3.6%	11.3%	0.2%
Files used for Random-Template (15)	2.6%	1.4%	11.9%
Randomly selected images (50)	1.9%	2.5%	5.9%

Table 2: Average correlation coefficients between the three templates and the files that were used to create them as well as the average correlation between each template and fifty randomly selected files.

quite preliminary; as such, additional work will be conducted on this before conclusions are made. Furthermore, these techniques will be used with quantitative planar 3-D velocity data in the not-to-distant future.

Summary

This work presented the progress made in relating the noise generation of an ideally expanded Mach 1.3 jet with a Reynolds number of 1.08×10^6 to the dynamics of the turbulence structures in its mixing layer. The work had three main components. The first was the calibration of the 3-D microphone array, which is used to locate the apparent sources of individual sound peaks recorded in the time domain. The second part dealt with the conditional sampling of the acoustic data in the time domain at 30° and at 90° . Finally, a preliminary investigation of simultaneously acquired flow / acoustic data using POD to determine what is occurring within the jet during sound generation was presented.

The calibration of the 3-D microphone array incorporated two small noise generating devices. The first was a plasma arc that was used to create acoustic tones for frequencies up to 20 kHz, while the second was a small fluidic device (HTFA) that was operated at three different conditions based on the resulting far acoustic field (two resonating and one broadband case). By examining the standard deviation of the calculated acoustic sources for the plasma arc and comparing them to the known location, the array was determined to be accurate for frequencies up to 10 kHz. The array was then used to locate the HTFA by measuring where the acoustic radiation was emanating. Based on these results, this 3-D array configuration can accurately locate noise sources with frequencies below 10 kHz.

Conditional sampling of the acoustic data at 30° and at 90° yielded two phase-averaged waveforms. This analysis was based on analyzing acoustic peaks that were above a set number of standard deviations of the respective signals. The waveform for the 90° location differed from that at 30° in a lack of side lobes and a much narrower shape. The lack of side-lobes leads to a flat frequency spectrum (typical of the 90° location) while the narrower shape is a result of the shorter time

scale of the turbulence that is radiating in this direction (as compared to the 30° location). Furthermore, the acoustic waveforms are similar in shape to the autocorrelations of the respective acoustic data. The conditional sampling also led to the observation that the acoustic radiation at 90° does not have prolonged periods of relative quiet as were observed in the 30° direction.

A preliminary Proper Orthogonal Decomposition (POD) analysis was performed on flow images that were simultaneously acquired with the acoustic source data from the 3-D microphone array (400 sets of data were available for analysis). Three types of flow images were analyzed based on the 3-D array data: 1) those where the array indicates that noise generation occurred during the flow image in a set region, 2) those where the top and bottom of the array were recording a prolonged period of relative quiet during the acquisition of a flow image, and 3) randomly selected flow images. Using the first two POD modes, the images within each of the three sets were reconstructed and then ensemble averaged to create the three templates shown in Figures 19 through 21. These templates were then cross-correlated to the flow images that were used to create them as well as additional randomly selected images. These correlation values were then averaged based on their category (twelve in all). The largest correlation values were between the templates and the images that were used in their creation. The lowest values were between the random templates and the files used to create the other templates. This analysis was very preliminary and future work will expand on it.

Acknowledgment

This work is sponsored by the Air Force Office of Scientific Research with Dr. John Schmisser as the Technical Monitor. The first, second, and third authors would like to thank the sponsors of the Ohio Space Grant Consortium Doctoral fellowship, DAGSI fellowship, and the Department of Defense for his National Defense Science and Engineering Graduate fellowship, respectively.

References

1. M.J. Lighthill, "On Sound Generated Aerodynamically: I. General Theory," *Proc. Royal Soc. London, Ser. A.*, Vol. 211, pp. 564-581, 1952.
2. G.L. Morrison, and D.K. McLaughlin, "Noise Generation by Instabilities in Low Reynolds Number Supersonic Jets," *Journal Sound and Vibration*, Vol. 65, pp. 177-191, 1979.
3. J. Stromberg, D. McLaughlin, and T. Troutt, "Flow field and acoustic properties of a Mach number 0.9 jet at a low Reynolds number," *Journal of Sound and Vibration*, Vol. 72, No. 2, pp. 159-176, 1980.
4. V. Sarohia and P.F. Massier, "Experimental Results of Large-scale Structures in Jet Flows and Their Relation to Jet Noise Production," AIAA Paper 77-1350, 1977.
5. D.F. Long, H. Kim and R.E.A. Arndt, "Controlled Suppression or Amplification of Turbulent Jet Noise," *AIAA Journal*, Vol. 23, No. 8, pp. 28-833, 1985.
6. J. Panda and R.G. Seaholtz, "Experimental Investigation of Density Fluctuations in High-Speed Jets and Correlation with Generated Noise," *Journal of Fluid Mechanics*, Vol. 450, pp. 197-130, 2002.
7. J. Hileman, B. Thurow and M. Samimy, "Exploring noise sources using simultaneous acoustic measurements and real-time flow visualizations in jets" *AIAA Journal*, Vol. 40, No.12, pp. 2382-2392, 2002.
8. J. B. Freund and T. Colonius, "POD Analysis of Sound Generation by a Turbulent Jet," AIAA Paper 2002-0072, 2002
9. E. Caraballo, M. Samimy, S. Narayanan, J. DeBonis and J. Scott, "Application of Proper Orthogonal Decomposition to a High Speed Axisymmetric Jet," AIAA Paper 2001-2783, 2001.
10. M. Glauser and W. George, "An Orthogonal Decomposition of the Axisymmetric Jet Mixing Layer Utilizing Cross-wire Velocity Measurements," *Proceedings of the 6th Symposium on Turbulent Shear Flows*, Toulouse, France, September 1987.
11. M. Glauser, X. Zheng and W. George, "The Streamwise Evolution of Coherent Structures in the Axisymmetric Jet Mixing Layer." *Symposium on Recent Developments in Turbulence*. pp. 207-221, 1990.
12. J. Citriniti and W. George, "Reconstruction of the Global Velocity Field in the Axisymmetric Mixing Layer Utilizing the Proper Orthogonal Decomposition," *Journal of Fluid Mechanics*, Vol. 418, pp. 137-166, 2000.
13. L. Ukeiley and J. Seiner, "Examination of Large Scales Structures in a Transonic Jet Mixing Layer," *Proceedings of FEDSM '98*, Washington, DC, 1998.
14. G. Kopp, J. Ferre and F. Giralt, "The Use of Pattern Recognition and Proper Orthogonal Decomposition in Identifying the Structure of Fully-Developed Free Turbulence," *Journal of Fluids Engineering*, Vol. 119, pp. 289-296, 1997.
15. J. Hileman and M. Samimy, "Turbulence structures and the acoustic far-field of a Mach 1.3 jet," *AIAA Journal*, Vol. 39, No. 9, pp. 1716-1727, 2001.
16. J. Hileman, B. Thurow and M. Samimy, "Acoustic Source Localization Using a 3-D Microphone Array in a Mach 1.3 Jet," AIAA Paper 2002-0366, 2002.
17. J. Hileman and M. Samimy, "Effects of Vortex Generating Tabs on Noise Sources in an Ideally Expanded Mach 1.3 Jet," AIAA Paper 2002-2482, 2002.
18. B. Thurow, J. Hileman, M. Samimy and W. Lempert, "Progress towards Real-time Planar Doppler Velocimetry," AIAA Paper 2003-0916, 2003.
19. B. Thurow, J. Hileman, M. Samimy and W. Lempert, "A technique for real-time visualization of flow structure in high-speed flows," *Physics of Fluids*, Vol. 14, No. 10, pp. 3449-3452, 2002.
20. J. Kastner and M. Samimy, "Development and characterization of Hartmann tube based fluidic actuators for high-speed flow control," *AIAA Journal*, Vol. 40, No. 40, pp. 1926-1934, 2002.
21. G. Raman, V. Kibens, A. Cain and J. Lepicovsky, "Advanced actuator concepts for active aeroacoustic control," AIAA Paper 2000-1930, 2000.
22. J. Hartmann and B. Trolle, "A new acoustic generator: the air-jet generator" *Journal of Scientific Instruments* Vol. 4, pp. 101-111, 1927.
23. M.J. Fisher, M. Harper-Bourne and S.A.L. Glegg, "Jet Engine Source Location: The Polar Correlation Technique," *Journal Sound and Vibration*, Vol. 51, No. 1, pp. 23-54, 1977.
24. K.K. Ahuja, K.C. Massey and M.S. D'Agostino, "A Simple Technique of Locating Noise Sources of a Jet Under Simulated Forward Motion," AIAA Paper 98-2359, 1998.
25. J. Simonich, S. Narayanan, T.J. Barber, and M. Nishimura, "Aeroacoustic Characterization, Noise Reduction, and Dimensional Scaling Effects of High Subsonic Jets", *AIAA Journal*, Vol. 39, No. 11, pp. 2062-2069, 2001.

26. J. Bridges and F. Hussain, "Effects of Nozzle Body on Jet Noise," *Journal of Sound and Vibration*, Vol. 188, No. 3, pp. 407-418, 1995.
27. S.K. Tang and N.W.M. Ko, "A Study on the Noise Generation Mechanism in a Circular Air Jet," *Journal of Fluids Engineering*, Vol. 115, No. 3, pp. 425-435, 1993.
28. O. Inoue, "Sound generation by the leapfrogging between two coaxial vortex rings," *Physics of Fluids*, Vol. 14, No. 9, pp. 3361-3364, 2002.
29. L. Sirovich, "Turbulence and the Dynamics of Coherent Structures, Part I, II, III: Coherent Structures," *Quarterly of Applied Math*, Vol. XLV, No. 3, pp. 561-590, 1987.
30. E. Caraballo, M. Samimy and J. DeBonis, "Low Dimensional Modeling of Flow for Closed Loop Flow Control," AIAA Paper 2003-0059, 2003.